Electric field-induced reversible trapping of microtubules along metallic glass microwire electrodes

Kyongwan Kim, Aurélien Sikora, Koji S. Nakayama, Mitsuo Umetsu, Wonmuk Hwang, and Winfried Teizer

Citation: Journal of Applied Physics **117**, 144701 (2015);
View online: https://doi.org/10.1063/1.4917203
View Table of Contents: http://aip.scitation.org/toc/jap/117/14
Published by the American Institute of Physics

Articles you may be interested in

Functional localization of kinesin/microtubule-based motility system along metallic glass microwires
Applied Physics Letters **105**, 143701 (2014); 10.1063/1.4896964

Electric field-induced reversible trapping of microtubules along metallic glass microwire electrodes

Kyongwan Kim,[1] Aurélien Sikora,[1] Koji S. Nakayama,[1] Mitsuo Umetsu,[1,2]
Wonmuk Hwang,[3,4,5] and Winfried Teizer[1,4,6,a)]
[1]*WPI-Advanced Institute for Materials Research (AIMR), Tohoku University, Sendai 980-8577, Japan*
[2]*Department of Biomolecular Engineering, Graduate School of Engineering, Tohoku University, Sendai 980-8579, Japan*
[3]*Department of Biomedical Engineering, Texas A&M University, College Station, Texas 77843-3120, USA*
[4]*Materials Science and Engineering, Texas A&M University, College Station, Texas 77843-3003, USA*
[5]*School of Computational Sciences, Korea Institute for Advanced Study, Seoul 130-722, South Korea*
[6]*Department of Physics and Astronomy, Texas A&M University, College Station, Texas 77843-4242, USA*

(Received 4 December 2014; accepted 22 March 2015; published online 9 April 2015)

Microtubules are among bio-polymers providing vital functions in dynamic cellular processes. Artificial organization of these bio-polymers is a requirement for transferring their native functions into device applications. Using electrophoresis, we achieve an accumulation of microtubules along a metallic glass ($Pd_{42.5}Cu_{30}Ni_{7.5}P_{20}$) microwire in solution. According to an estimate based on migration velocities of microtubules approaching the wire, the electrophoretic mobility of microtubules is around 10^{-12} m^2/Vs. This value is four orders of magnitude smaller than the typical mobility reported previously. Fluorescence microscopy at the individual-microtubule level shows microtubules aligning along the wire axis during the electric field-induced migration. Casein-treated electrodes are effective to reversibly release trapped microtubules upon removal of the external field. An additional result is the condensation of secondary filamentous structures from oriented microtubules. © *2015 AIP Publishing LLC*. [http://dx.doi.org/10.1063/1.4917203]

I. INTRODUCTION

Microtubules (MTs) are dynamic structural elements responsible for cell evolution in shape and polarity during the cellular differentiation.[1] They are also involved in the intracellular cargo transportation as tracks for motor proteins, for example, kinesin.[2] Successful reconstruction of such subcellular dynamic parts in *in vitro* environments[3,4] has made various visionary goals feasible: utilization of their native functions in nanotransport devices,[5,6] table-top studies of pattern formation in systems of self-driven components,[7–10] and elucidation of new functions for bio-electronic device development.[11,12] Spatio-temporal organization of the bio elements is arguably a crucial requirement in device applications as it is vital for cell survival. A variety of approaches has achieved spatial arrangements of the reconstructed biomolecules to confine their motional activities within predefined areas.[13–18] On the other hand, translocation and orientation of MTs suspended in solution have been achieved by using electric fields.[19–23] A MT consists of tubulin dimer subunits (heterodimers each consisting of an α-tubulin monomer and a β-tubulin monomer with dimer dimensions of 46 Å × 80 Å × 65 Å). Longitudinal head-to-tail coupling of the subunit proteins forms protofilaments. Lateral binding of the protofilaments leads to the tubular filamentous MT structure. Typically, 13 protofilaments are coupled in a single MT, resulting in an outer diameter of 25 nm.[24,25] Based on the typical microtubule length (several μm) and the periodic nature of the MT structure, any net electrostatic parameter of a single tubulin subunit, such as charge or dipole moment, results in a corresponding value of considerable magnitude for a MT. For example, the number of tubulin dimers in a 10 μm long MT is about 16 000. This leads to substantial electrostatic interactions between MTs.[26]

Micro/nano-patterned areal electrodes have been used for reversible aggregation of MTs along the electrode geometry[27] and for spatio-temporal controls of the *in vitro* motility.[21,28,29] Envisioning additional flexibility in bio/nano-device applications, we recently directed our attention towards the use of wire type tracks for the kinesin/MT-based bio-molecular transport system.[30–32] As explained earlier, traditional methods rely on patterned tracks which are permanently defined on a two-dimensional substrate.[13–18] Wire tracks can localize the activity of bio-molecules similar to the traditional approach, yet the wires are independent entities, thus reconfigurable even in three-dimensional space, unlike fixed planar tracks. Here, we focus on electrical control of MTs by employing $Pd_{42.5}Cu_{30}Ni_{7.5}P_{20}$ metallic glass (Pd-MG) in the form of wires with several micrometers in diameter and a centimeter in length.[33,34] The superior functionalities of metallic glass, including ultrahigh strength, low Young's modulus, chemical activity, soft magnetism, and thermo-plastic formability, are suitable for flexible designs of functional structures in micro/nano devices. Recently, large-scale production of metallic glass micro- and nanowires has been achieved by adapting a conventional gas atomization process.[33] Metallic properties of the wires allow the temporal formation of electric fields. Moreover, we have verified the compatibility between the particular metallic

a)E-mail: teizer@physics.tamu.edu. Telephone: 1-979-845-7730. Fax: 1-979-845-2590.

 © 2015 AIP Publishing LLC

glass microwire and the kinesin/MT-based motility. Thus, the Pd-MG microwire readily becomes a suitable "metallic" substitute for a non-conducting glass wire, while carrying out additional functions, most importantly serving as an electrode for the application of an electric field. Besides the advantage from flexible electrodes, the long wire geometry is favorable for aligning MTs along the wire axis as will be discussed below. This conductive wire-based approach to align MTs along an intended direction is straightforward in comparison to the previous methods requiring either high magnitude AC-fields or nano-fabrication.[22,23,27,35] Linearly organized MTs are necessary for efficient molecular sorting and delivery, particularly for a long distance delivery beyond the typical length scale of a single MT. Furthermore, artificial bundling of MTs along a linear template may be applicable in construction of model cellular structures, such as axons and tunneling nanotubes.[36,37] Also, the level of order of intracellular components, correlated with local electric fields, may play an important role in pathogenic mechanisms of diseases such as cancer and Alzheimer's disease.[38,39]

II. MATERIAL AND METHODS

The Pd-MG wires were produced in a custom-built gas atomization system.[34] $Pd_{42.5}Cu_{30}Ni_{7.5}P_{20}$ alloy was used because it has a high glass forming ability and a high spinnability to form fibers. About 3 g of Pd-MG was cut and heated in a crucible by an induction heating system. The heating temperatures were monitored by an optical pyrometer with the emissivity of 0.50, which was calibrated at the Al melting point. After being heated above its melting point ($T_m = 803$ K), Pd-MG was supercooled by 10 K. The melt stream was then extruded through the crucible nozzle by the Ar injection pressure of 0.05 MPa, and was then atomized by an Ar jet with a pressure of 10 MPa. The jet fragmentation of the melt stream leads to ligament formation and the elongation of ligaments allows the formation of fine fibers. The produced MG wires have a distribution with the range of 50 nm–5 μm in diameter and 10 μm–1 cm in length.

The layout of a complete device is described in Figure 1. Pieces of conductive double-sided tape (Teraoka Tape) were affixed on a glass slide (S2111, Matsunami). Electrodes were defined by cutting the tape using a razor blade. Top glue layers of the tapes were peeled off. Revealed metal surfaces were cleaned using kimwipes soaked with acetone. A flow cell including two counter electrodes was defined by paraffin film (Parafilm M: Pechiney Plastic Packaging). A strand of Pd-MG microwire was put on the parafilms crossing the flow channel. The flow channel was then closed by a glass coverslip (18 mm × 18 mm, thickness No. 1, Muto Pure Chemical). The coverslip was gently pressed down while the whole device was held at T = 80 °C on a hot plate. The Pd-MG microwire and additional copper wires were then electrically connected to the electrodes by cold-pressed indium.

The MT solution was prepared by a conventional method.[40] A frozen (at −80 °C) tubulin mixture (5 mg/ml in PEM buffer (80 mM PIPES, 1 mM EGTA, 1 mM $MgCl_2$, pH 6.9 controlled by NaOH) with 1 mM GTP and 6% (v/v) glycerol, ratio of unlabeled tubulin (T240, Cytoskeleton) to

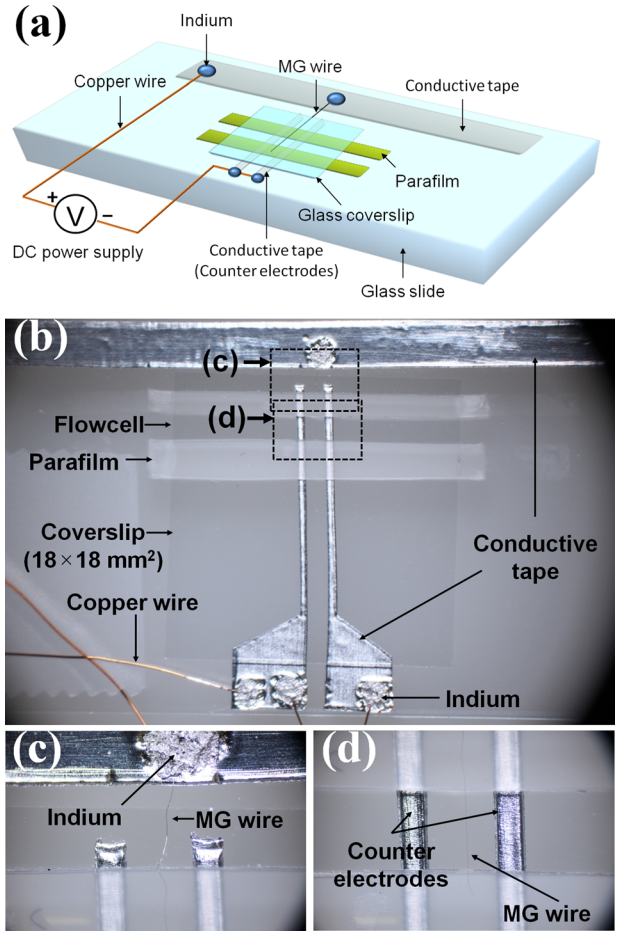

FIG. 1. (a) Schematic three-dimensional diagram of the device layout. (b) Photograph of the device. Photographs for the core region of the device (black dotted rectangle in (b)), (c) outside the flow cell and (d) inside the flow cell.

rhodamine-labeled tubulin (TL590M, Cytoskeleton) ~7:3) was incubated for 15 min at 37 °C. After incubation, the tubulin solution was diluted 200 fold by PEM buffer, which contains 10 μM taxol (T7402 Paclitaxel, Sigma-Aldrich) for MT stabilization. The MT solution was further diluted (10 folds) in PEM buffer containing a typical antifade system (20 μg/ml glucose oxidase, 8 μg/ml catalase, 20 mM glucose, 0.5% (v/v) β-mercaptoethanol) and 10 μM taxol for fluorescence microscopy.

After filling a casein-treated flow cell (note the next paragraph) with the prepared MT solution, the two entrances of the cell were sealed with VALAP (Vaseline-Lanolin-Paraffin), and the device was mounted in a fluorescence microscope (IX-71, Objective lens-UPlanFL 40×, Olympus) equipped with a CCD camera (ImagEM, Hamamatsu, Adaptors: U-TV1XC and U-PMTVC4XIR) and filter set (XF204, Omega Optical). Note that the coverslip side is facing down to the lens of the microscope. Thus, the wire electrode lies between the counter electrodes and the objective lens. A DC-power supply (AD-8723D, As One) was connected to the electrodes via the copper wires as depicted in Figure 1(a).

Direct exposure of the Pd-MG wire to the MT solution leads to fouling of MTs on the surface. In order to avoid such undesirable events, the wire, in addition to the entire

flow cell, was coated with casein which passivates the surface.[27] The casein coating was the result of introducing casein solution (Casein 037–20815, Wako Pure Chemical Industries, 1 mg/ml in PEM buffer) into the flow cell and incubating for 10 min at room temperature.

III. RESULTS AND DISCUSSION

A. Electric field control of the local density of MTs

Figures 2(a)–2(h) (Multimedia view) show fluorescence microscopy images of the MT distribution in the buffer solution, which depends on the applied DC voltage. The two movies were acquired on the same region containing a Pd-MG microwire electrode while a series of voltage pulses (t = 3 min) were applied. The observation was separated into two movies because the number of frames per recording is limited by the software. The time gap between the two movies was about 3 min. The voltage was set to zero for 3 min after each pulse. The images (Figures 2(a)–2(h) (Multimedia view)) were acquired 20 s before turning on/off the pulses, respectively (see below). At a voltage of 2.1 V, the MTs around the electrode appear weakly attracted to the electrode (black vertical line). At larger voltage, it becomes clearer that the motion of MTs towards the electrode is in response to the voltage pulses. This attractive motion is triggered by an electrostatic interaction between the MT having negative effective charge in the buffer solution and the wire electrode acting as an anode in the experimental setup. Upon turning off the applied voltage, the MTs diffuse back into the solution. The diffusive motion does not suffice to return the MT distribution to its initial homogeneity after 3 min. An elevated MT population density is seen around the wire right before the next pulse is applied. This is a remnant of the previous trapping cycle, an effect which is more obvious at higher pulse amplitude.

As MTs are stacked or bundled on the wire during the trapping process, we quantify the trapped MTs by analyzing the mean intensity near the wire electrode. Each frame (exposure time: 360 ms) is converted to a grey scale image. The wire electrode in each frame is defined by a rectangle at a

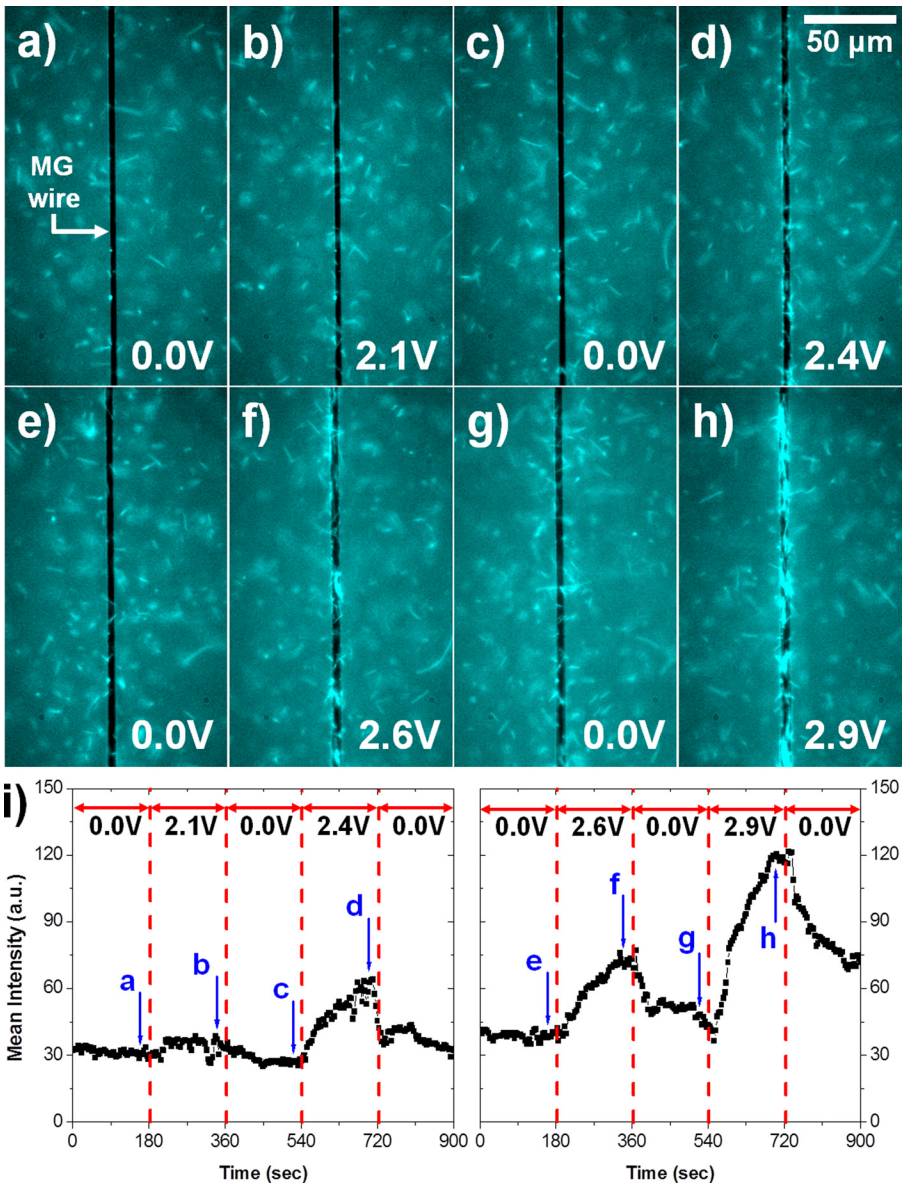

FIG. 2. Reversible electrophoretic accumulation of microtubules onto a Pd-MG microwire. (a)–(h) Fluorescence and bright-field images show the voltage dependent distribution of microtubules in a flow cell. Numbers are applied voltages in volts (V). The scale bar (in (d)) indicates 50 μm. Time (top right, in min:s) is tagged in each frame of multimedia view. (i) The mean intensity measured on the Pd-MG microwire as a function of time (obtained from two separate movies: Multimedia view of (a)–(d) (left plot) and (e)–(h) (right plot). A software limitation of the number of frames per recording required two movies which have a time gap of ~3 min). Numbers on top of each graph are voltages applied during the time intervals indicated by the vertical dotted lines. The moments for the figures (a)–(h) are marked on the graphs with arrows. (Multimedia view) [URL: http://dx.doi.org/10.1063/1.4917203.1][URL: http://dx.doi.org/10.1063/1.4917203.2]

constant pixel area (5090: $\sim 4\,\mu m \times 204\,\mu m$) and the mean intensity of the defined region is calculated using ImageJ, an open access software for image analysis (available at http://imagej.nih.gov/ij/). The mean intensity is plotted in Figure 2(i) (Multimedia view) as a function of time (two diagrams show results obtained from the two separate movies: Multimedia view of Figures 2(a)–2(d) (left plot) and Figures 2(e)–2(h) (right plot)). The moments when the images in Figures 2(a)–2(h) (Multimedia view) were acquired are indicated with arrows on the graph. The mean intensity changes in correlation with the pulse pattern. An increase of trapped MTs at higher voltage is observed in each plot. In our particular electrode configuration, the degree of response of MTs in the electrophoretic motion is not uniform but gradually decays in the radial direction from the wire. As an estimate, we use a simplified electrostatic model treating the buffer solution as a linear dielectric medium, which qualitatively explains the observations. Electrodes are approximated as an infinite cylindrical conductor (one of the counter electrodes) and an infinite line charge (the MG wire) aligned in parallel to each other. By the method of image charges,[41] the electric field at a point on the line perpendicularly connecting the cylindrical conductor with the line charge is proportional to $(r^{-1} + (l - r)^{-1})$, where r is the radial distance from the line charge pointing toward the center of the cylindrical conductor and l is the radial distance to the image line charge ($l = (l_0^2 - R^2)/l_0$, here l_0 is the center-to-center distance between the two electrodes and R is the radius of the cylindrical conductor.). We consider a situation similar to the arrangement of the electrodes in the presented device. The bar-shaped counter electrode is treated as a conducting cylinder with R of $200\,\mu m$ and l_0 is chosen to be $900\,\mu m$ (see Figure 1(b)). In this situation, the field strength at $r = 20\,\mu m$ is $\sim 25\%$ of the value at $r = 5\,\mu m$. The distance between the wire and the counter electrode is large enough to ignore the second term of the formula for the electric field within the range of distances considered here. Electrophoretic migration velocities of MTs are linearly proportional to the electric field strength.[19,20] Thus, the distance dependent ($\sim r^{-1}$) electric field formed by the wire electrode leads to the spatial inhomogeneity of the electrophoretic movements of MTs. Such a drop of the field strength in the proximity of the wire qualitatively agrees with our observations (note the $50\,\mu m$ scale bar in Figure 2(d) (Multimedia view)). MT motions responding to the voltage pulse, i.e., toward the electrode, gradually subside as the distance from the wire increases.

In order to characterize the electric field-induced MT movement, we traced individual MTs moving around the wire electrode while electric potentials were applied. The x-coordinates (perpendicular to the wire axis) of several MTs in image frames of the movie, Figures 2(e)–2(h) (Multimedia view), are plotted in Figures 3(a) and 3(b) as functions of time (interval of 5 s) for two different applied potentials, 2.6 V and 2.9 V, respectively. Here, the coordinate indicates the center of mass of the MT, as measured by ImageJ. There are two reasons that lead to challenges in tracking MTs, therefore, limiting our sampling of MTs (34 and 33 MTs were sampled for the applied potentials 2.6 V and 2.9 V, respectively). First, MTs in our experiments are not moving within a single focal plane unlike in the case of MTs in a two-dimensional chamber.[20] Second, the electrophoretic force in our experiments is comparably weak, as it will be discussed below. These factors lead to strong fluctuation of MTs in three-dimensional space. As a result, MTs are often going out of focus, overlapping with each other, or even completely disappearing out of view as time passes. The MTs we sampled for this analysis are those that can confidently be tracked. Each line connecting a group of data points (color online) represents the change in location (x-coordinate) of an individual MT with time. Gray horizontal bars ($x \approx 97\,\mu m$) are added in the plots to mark the location of the wire electrode. As expected, the lines for MTs in proximity of the wire indicate that MTs are attracted toward it, and the overall motion trend is symmetrical with respect to the wire axis. A surprise is the appearance of MTs apparently moving away from the wire. First, we consider a simple picture modelling only the electrophoretic response of MTs to an electric field, which decays with radial distance (r) as $\sim r^{-1}$. Since the wire lies in the observation plane, the distance in x between a MT and the wire axis is a measure of the radial distance. Assuming that the local drift velocity (dx/dt) of a MT is proportional to the electric field strength, i.e., $dx/dt = \alpha x^{-1}$, the x-coordinate of a MT at time t is written as, $x(t) = (x_0^2 - 2\alpha t)^{1/2}$. Here, α is a proportionality constant and x_0 is the x-coordinate at $t = 0$. x-t curves with several different initial distances are shown in Figure 3(c) for the case of $\alpha = 2$ as an example. These curves exhibit MTs approaching the wire ($x = 0$), a resemblance to the experimental results. However, this model fails to reproduce the outward motion of MTs. Such motion will require an additional flow field that must be repulsive (outward from the wire) with strength comparable to the electrophoretic attraction. We consider an electro-osmotic flow as a possible candidate for a repulsive flow field.[20,42] Electro-osmotic flows are created by responses of mobile positive ions gathered on glass surfaces to external electric fields. Thus, the flow direction is opposite to that of the electrophoretic motion of MTs whose effective charges are negative. To qualitatively understand the influence of the electro-osmotic flow, we assume that the flow velocity is proportional to the tangential component of electric field (E_t) measured at the coverslip surface. In our experimental setup, E_t varies with the distance x as $\sim x/(x^2 + d^2)$, here d is the shortest distance between the wire axis and the coverslip surface (assuming that the wire axis is parallel to the surface). Adding this term, one arrives at a net velocity field, $v_{net} = -\alpha x^{-1} + \beta x(x^2 + d^2)^{-1}$. Here, β is a coefficient and a minus sign indicates a direction toward the wire. Integration of this equation produces characteristic curves representing the net motion of MTs. Resulting curves with several different initial distances are plotted in Figure 3(d) for the constants, $d = 40$, $\alpha = 7$, and $\beta = 18$ as an example. These numbers constitute a combination that produces a transition in the motion direction (see below) at $x \sim 30\,\mu m$, similar to the experimental results (markers put on the regions $\sim 30\,\mu m$ above/below the wire in Figures 3(a) and 3(b)). In taking account of an electro-osmotic flow, this approach can thus explain the emergence of the repulsive zone in which MTs

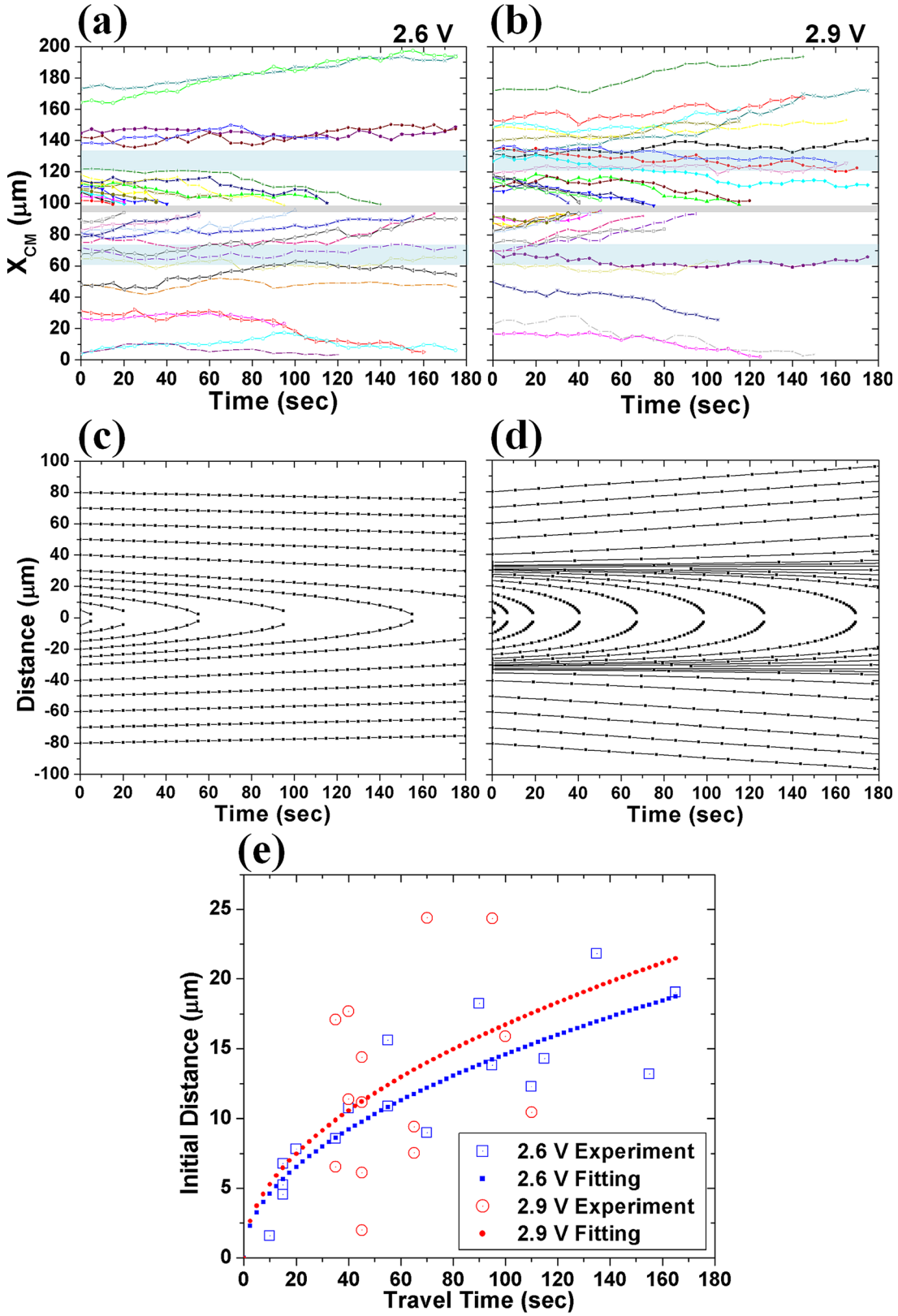

FIG. 3. (a) and (b) Time evolution of x-coordinates (center of mass) of MTs moving near a Pd-MG wire electrode while electric potentials ((a) 2.6 V and (b) 2.9 V) were applied. The gray bar ($x \approx 97\ \mu$m) on each panel indicates the location of the wire. Each line connecting the same symbols (color online) traces an individual MT. (c) Time evolution of the distance (x) between a charged object and a wire electrode using a model considering electrophoretic movement only. The motion velocity is given by $-\alpha x^{-1}$. The presented curves are for the case of $\alpha = 2$ with several initial distances. (d) Time evolution of the distance (x) between a charged object and a wire electrode using a model including a counter flow. The motion velocity is given by $-\alpha x^{-1} + \beta x(x^2 + d^2)^{-1}$. The presented curves are for the case of $\alpha = 7,\ \beta = 18,$ and $d = 40$ with several different initial distances. (e) Initial distances (x_0) of MTs versus the time required for the MTs to reach the wire. The large empty symbols indicate the experimental results (blue squares for 2.6 V and red circles for 2.9 V). The small filled symbols model curves of $x_0 = \sqrt{2\alpha t}$ with the best-fit values of α (1.064 μm^2/s for 2.6 V (blue squares) and 1.397 μm^2/s for 2.9 V (red circles)).

avoid approaching the wire electrode. MTs with initial distances larger than a critical value ($x_c = d\{\alpha/(\beta - \alpha)\}^{1/2}$, which is the distance where the net velocity becomes zero) move away from the wire. Meanwhile, MTs with initial distances smaller than the critical value collapse onto the wire eventually.

A rough estimation of the electrophoretic mobility of MTs is performed based on the electrophoretic motion-only case for simplicity. The mobility (μ) is defined as a proportional coefficient in the relationship between velocity and electric field, i.e., $\vec{v} = \mu\vec{E}$. Electric field strength at a distance x is given by, $E(x) \sim -V/\{\ln(a/h) \cdot x\}$. Here, V is the electric potential on the wire, a is the radius of the wire, and h is the distance between the wire and the counter electrode. Since we have set $v = -\alpha/x$ (here again, a minus sign indicates a motion direction toward the wire electrode), we can write $\mu E(x) = -\alpha/x$, and therefore, $\mu = \{\alpha\ln(a/h)\}/V$. The coefficient α is estimated from the experimental results. For this, the initial distances (x_0) of MTs are plotted as a function of travel time in Figure 3(e) (blue empty squares for 2.6 V, red empty circles for 2.9 V). Here, the travel time is the time required for the MT to reach the wire. The little filled blue squares and red circles represent the equation, $x_0 = \sqrt{2\alpha t}$, with the best-fit values of α, $1.064 \pm 0.116\,\mu m^2/s$ and $1.397 \pm 0.363\,\mu m^2/s$, respectively. From these values (with $a = 2.5\,\mu m$, $h = 900\,\mu m$), we find $\mu \sim -2.4 \times 10^{-12}\,m^2/Vs$ and $\sim -2.8 \times 10^{-12}\,m^2/Vs$ for 2.6 V and 2.9 V of the applied potential, respectively. The discrepancy between these two values could be due to the use of an incomplete model as well as the high fluctuation in the motion of MTs. More strikingly, these values are four orders of magnitude smaller than the mobility measured from previous studies based on an experimental set-up that consists of a fluidic channel between 5 and 50 mm sized reservoirs making contacts with electrodes.[19,20] We ascribe such a significant suppression of the mobility, seemingly common for near-electrode observations,[21] to screening by electrode polarization that leads to a large drop of the applied potential near the electrode.[43] A reduction of the effective charge of MTs by screening may be also taken into account in understanding these results.[21]

B. Electric field control of the local orientation of MTs

A specifically designed electrode can align MTs along the electrode geometry.[27] A narrowly constricted electrode provides charged objects with force fields converging toward the electrode. MTs in the vicinity of the electrode gradually approach the electrode, until complete binding to the electrode minimizes the electrostatic energy. Even though the wire diameter in our work is at least 200 times larger than that of a single MT, we observed MTs preferentially aligning along the wire axis. Figure 4 (Multimedia view) shows a series of fluorescence microscopy images selected from a movie acquired on a different device at higher magnification. Figures 4(a)–4(g) (Multimedia view) demonstrate MTs (marked with symbol-tagged colored arrows) aligning linearly along the wire axis during the electrophoretic migration

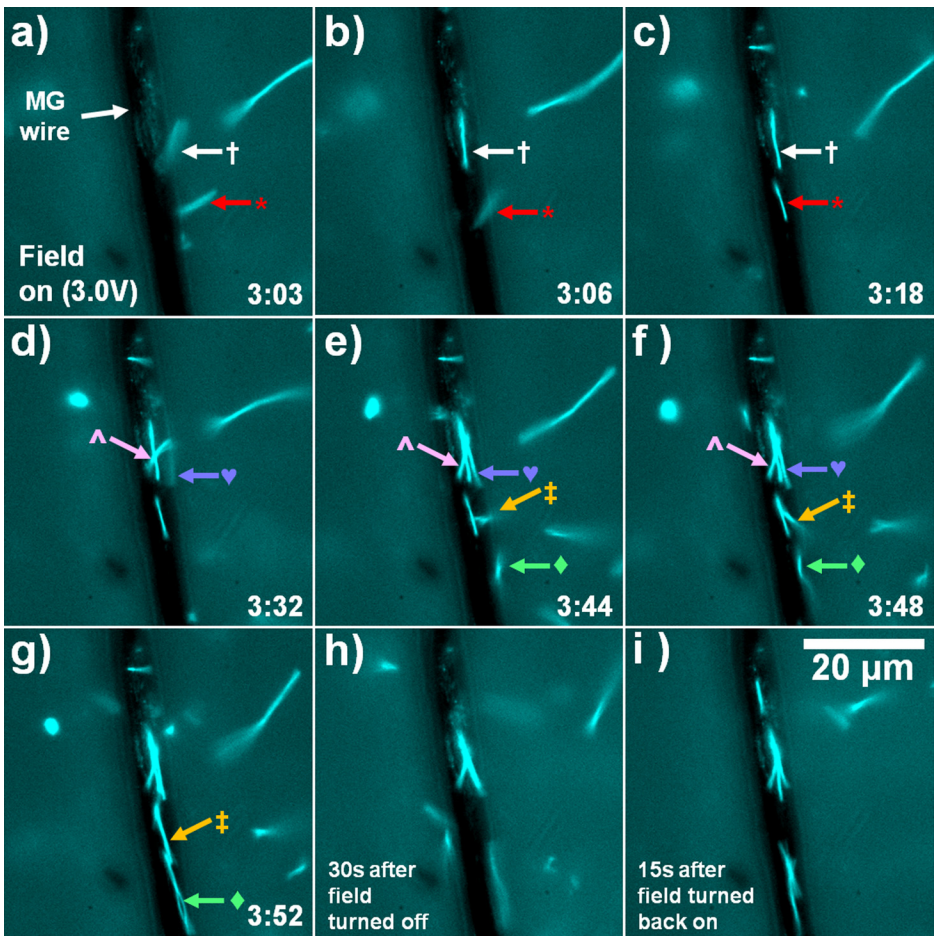

FIG. 4. Fluorescence and bright-field images of microtubules aligning along a Pd-MG microwire during electrophoretic migration. (a)–(g) Microtubules approaching to the wire electrode in 3.0 V pulse. Symbol-tagged colored arrows trace microtubules making a linear arrangement along the wire. Numbers are time (min:s). Voltages are tagged in each frame of multimedia view of Figure 4. (h) Microtubules around the wire 30 s after the field is turned off. (i) Microtubules re-aligned on the wire 15 s after the field is turned back on. The scale bar (in (i)) indicates 20 μm. (Multimedia view) [URL: http://dx.doi.org/10.1063/1.4917203.3]

in a 3.0 V pulse. The absolute time for each frame is tagged at the bottom right corner (in min:s). The electric field-induced alignment is achieved in a reversible manner as shown in Figures 4(h) and 4(i) (Multimedia view), indicating MTs around the wire 30 s after the field is turned off and 15 s after the field is turned back on, respectively.

We consider a simple argument based on the electrostatic interaction between a MT, a rigid rod, and an infinitely long wire of cylindrical symmetry. MTs near the wire are pulled toward the wire by electrophoretic migration. Upon landing on the surface of the wire, the MTs will be at particular orientations which are decided by the MTs' initial conditions (e.g., location, orientation, and length) and the field strength. Near the wire electrode, the electric field is approximately cylindrically symmetric. For instance, in the situation given above, i.e., a distance of 900 μm between the cylinder and the line charge, the electric potential is almost uniform along a cylinder encircling the line charge with a radius of 10 μm. The difference between the maximum and the minimum potential is within 1% of the minimum value. This increases up to about 5% when the distance between the cylinder and the line charge is 300 μm. The cylindrically symmetric electric field formed by the anodic wire electrode provides a MT, a negatively charged rod, with an anisotropic double-well potential energy, with two energy minima at the MT orientations parallel and anti-parallel to the wire axis. This anisotropy ultimately leads to a MT orientation along the wire axis, which is energetically most favorable.

The kinetics for the alignment process can be described by considering electrostatic force fields that trigger the electrophoretic rotational movements of MTs. A situation of a MT making contact with a wire (only the section of interest is emphasized) at an arbitrarily chosen orientation is shown in Figure 5(a). Due to the cylindrical symmetry of the electric field, all the forces exerted on infinitesimal segments of the MT are vertically pointing toward the centre line of the wire as drawn in Figure 5(b) (force vectors are drawn only for some arbitrarily chosen points representing the segments). Note that the force fields are drawn in the top-view schematic. In fact, all the segment points can have different z-components. In general, the forces are decomposed into two components orthogonal to each other. One is perpendicular ($\mathbf{F}_{pe}$: blue arrow) and the other is parallel ($\mathbf{F}_{pa}$: green arrow) to the MT projected onto the top-view plane. The two independent groups of force components are separately marked along the MT in Figures 5(c) (parallel) and 5(d) (perpendicular). The forces in Figure 5(d) generate a torque (τ_w) which rotates the MT about the wire axis until the net torque vanishes. The torque vector is indicated in Figure 5(c) at the contact point. The blue open circular arrow shows the direction of the rotation. Meanwhile, the forces in Figure 5(c) will generate a torque (τ_r) which rotates the MT about the radial axis defined at the contact point (the green open circular arrow showing the direction of the rotation). A finite torque exists until the MT is oriented precisely parallel to the wire axis. Here, we only focus on the rotational motion although the forces partly generate a translational motion along the MT axis as well. Putting all these rotational motions together, the final orientation of the MT will be the same as the wire axis in any case. One exceptional case is that the initial orientation of MT is precisely perpendicular to the wire axis. In such a case, no rotational force to orient MTs along the wire axis is generated. However, this situation constitutes an unstable equilibrium. The electrostatic energy is not the only factor which makes it unstable. In reality, while a MT approaches a contour of the minimum electrostatic energy, it is also changing its static energy arising from the bending of its body. The electrostatic equipotential plane is cylindrical. Therefore, it is probable that MTs, by virtue of thermal perturbation, avoid the unfavorable orientation perpendicular to the wire axis. In this simple picture, we neglected frictional forces which come from the physical contact of MTs with the casein-treated wire surface, ion charge distributions, and fluid dynamics, which provide more precise descriptions about the electric field profile and the electrophoretic mobility of MTs.[20] The frictional force (which is proportional to the electric field strength), together with the bending stiffness of the MT, is significant for determining the final MT orientation in a real situation. In the realistic situation, therefore, the final orientation of a MT on the surface of the wire electrode will depend on the electric field strength in a more complicated manner. Reversely, real time monitoring carried out with feedback control of the electric potential may allow delicate manipulation of the final orientation of an individual MT. Nevertheless, as is seen in our experimental results, the MT alignment with the wire axis is generally quite good,

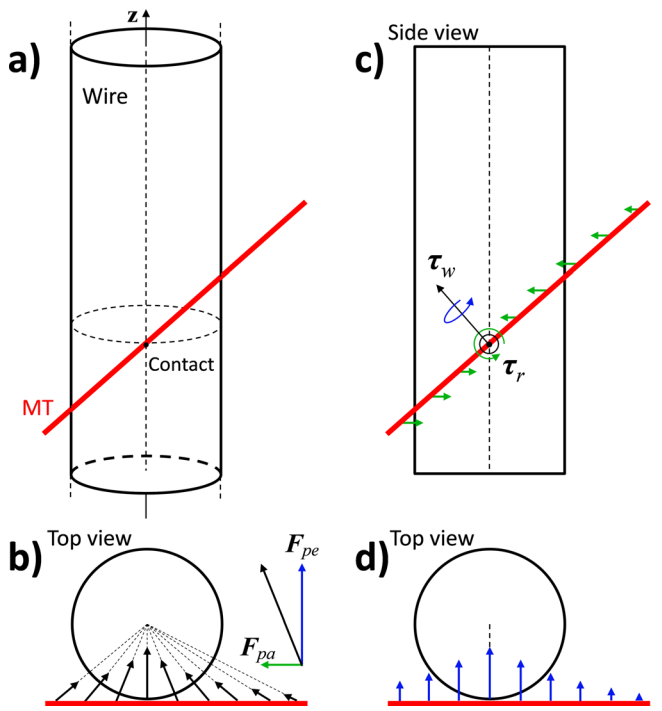

FIG. 5. (a) Schematic diagram of a microtubule making contact with a cylindrical wire electrode at an arbitrarily chosen orientation. (b) Top view of (a). The electrostatic force vectors are indicated along the microtubule projected onto the top-view plane. The force vector is decomposed into two components, perpendicular ($\boldsymbol{F}_{pe}$: blue arrow) and parallel ($\boldsymbol{F}_{pa}$: green arrow) to the microtubule projected onto the top-view plane (color online). (c) Side view of (a) indicating the perpendicular force components along the microtubule. (d) Top view of (a) indicating the parallel force components along the microtubule. Torque vectors generated by the two independent force groups are indicated at the contact point.

indicating that this simple model describes the experimental situation reasonably well.

Some of the trapped MTs are permanently fixed to the electrode. This is possibly due to either native defects in the passivating layer or surface damage by strong binding. Electric fields over a certain value affect the MT stability severely as also seen in previous studies.[19,23,27] In the particular case of the device presented here, the MTs trapped on the wire are destroyed when applying a 3.3 V pulse (Figure 4 (Multimedia view)). Whereas this is possibly due to alteration of buffer conditions during the electric excitation, the substantial external electrostatic force exerted on MTs near the electrode may also produce a direct effect on the stability of MTs, a polymer built based on electrostatic coupling (~1 eV) between tubulin subunits.[44,45] Further study to clarify this issue will be important for future applications. Weakly fixed (non-contact) MTs are seen to have freedom in the lateral motion on the wire, indicating the direction of the trapping force is indeed perpendicular to the surface.

C. Electric field-induced MT condensation

We observe an additional remarkable phenomenon, in that trapped MTs condense into a secondary filament by

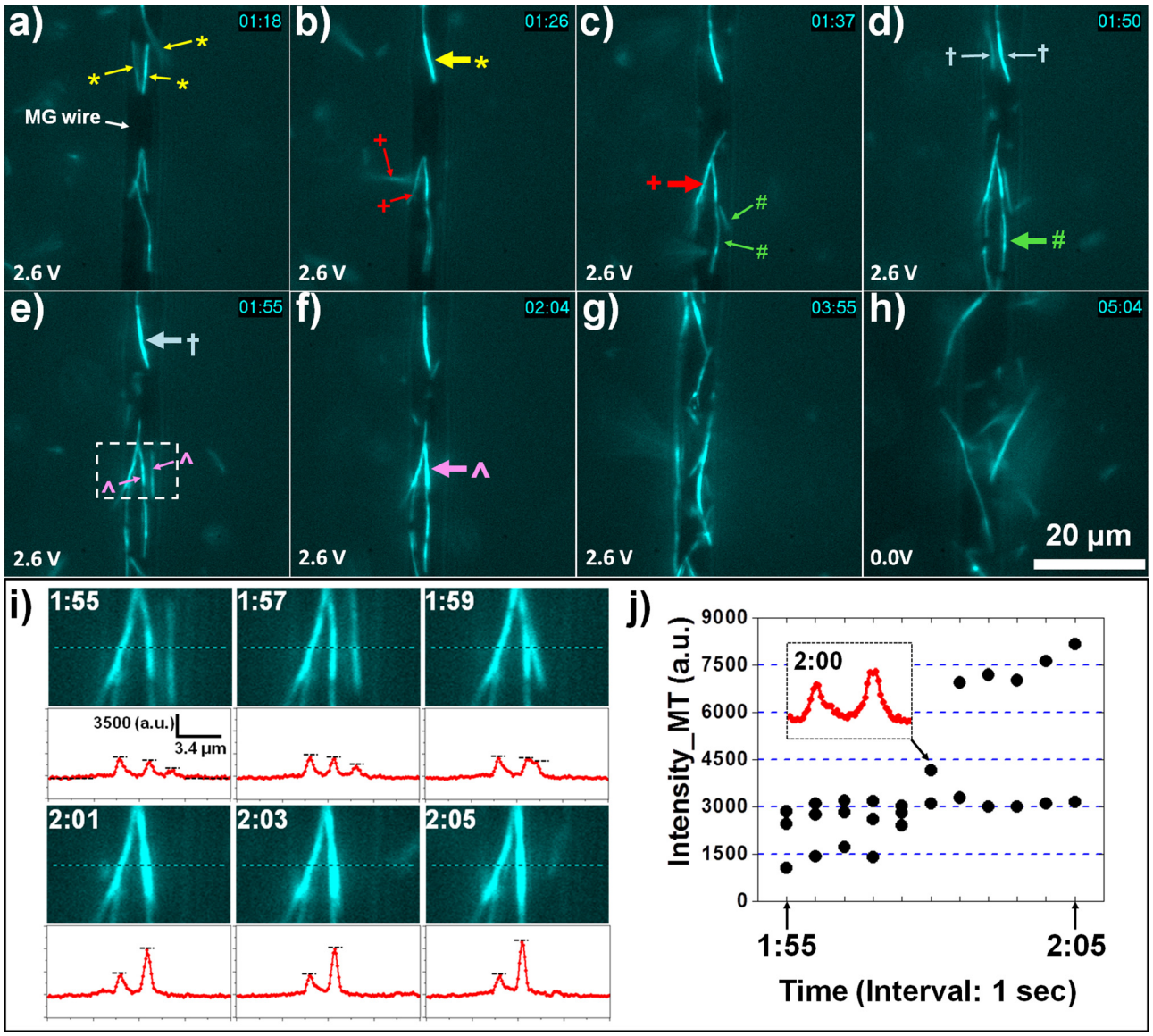

FIG. 6. Fluorescence and bright-field images of microtubules trapped on a Pd-MG microwire while voltage is applied (2.6 V). (a)–(f) MTs laterally bind to each other forming secondary filamentous structures as time (top right in min:s) increases. The symbol-tagged colored thin arrows point to MT-elements forming secondary filaments appearing in the next consecutive image (the resulting secondary filaments are indicated by a thick arrow with the same color and symbol). (g) MTs in the condensed structures in a different region about 5 s before the field is turned off. (h) The same region as in the panel (g) showing MTs diffusing away from the wire electrode in the absence of an external field (about 1 min after the field has been turned off). The scale bar (in (h)) indicates 20 μm. (i) Time course of MT condensation. Fluorescence images indicate MTs in the region defined with the white dotted rectangle in (e). The number in each image indicates time (min:s). The intensity profiles measured along the dotted line are shown below the images, respectively (vertical axis: intensity, horizontal axis: distance). Vertical (horizontal) scale bars in the first profile graph are 3500 in arbitrary unit (3.4 μm). Black dotted lines are added as guidelines. (j) The intensity of MTs (see the main text) plotted as a function of time (from 1:55 to 2:05 with intervals of 1 s). Inset: The intensity profile at time 2:00 showing the complete merging of two peaks, which had been separate before. (Multimedia view) [URL: http://dx.doi.org/10.1063/1.4917203.4][URL: http://dx.doi.org/10.1063/1.4917203.5]

laterally coupling with each other. A representative observation of the electric field-induced MT condensation is presented in Figure 6 (Figures 6(a)–6(f) and Figures 6(g) and 6(h) (Multimedia view), because of a frame size limitation.). Upon application of an electric field around a wire electrode, MTs are accumulated along the wire with a preferential orientation as already discussed. MTs marked by thin yellow arrows (tagged with asterisks) in Figure 6(a) (Multimedia view) are coupled in parallel and a secondary filament results, which is marked in Figure 6(b) (Multimedia view) by a thick yellow arrow (tagged with the same symbol). Several similar events are indicated by using different color-coded arrows (tagged with different symbols) through Figures 6(a)–6(f) (Multimedia view). We notice that the intensity of the resulting filament is enhanced as MTs condense into the filament. Snapshots showing different times of the MT condensation are arranged in Figure 6(i) (Multimedia view) with intensity profiles along the lines indicated in the snapshots. The enhancement of the intensity is obvious when two peaks have merged. The intensity distribution may serve as a measure to count MTs in a bundled structure. The intensity values of MT-filaments are defined by subtracting the background intensity (average intensity for the distance 0–3.4 μm and 10.2–13.6 μm, see the black-dotted guide lines in the first profile graph) from the peak values (Figure 6(j) (Multimedia view)). The graph shows a somewhat discrete intensity distribution. However, a simple addition of the values evidently fails to count MTs in the secondary filaments. Furthermore, in this particular case, counting MTs in bundles from the microscopy analysis may require extra care since the MTs are not moving on a flat surface, i.e., a single focal plane. The inhomogeneous intensity profile along the secondary filaments, a signature of laterally overlapping MTs, is maintained for a considerable amount of time even after the field is turned off, indicating that it is likely a consequence of physical coupling rather than a temporary overlap. The snapshot in Figure 6(h) (Multimedia view) shows some of the secondary filamentous structures diffused away from the wire electrode about 1 min after the field was turned off. The same region before the field was turned off is shown in Figure 6(g) (Multimedia view).

The trapped MTs are oriented and the trajectories of thermal motion of them are confined within the cylindrical surface of the wire due to the electric field. Such a situation favors MTs interacting with each other over a large length due to their quasi-one-dimensional nature. The probability of such a scenario may depend on the strength of the electric field that controls (1) the anisotropy barrier to orient MTs, (2) the degree of spatial confinement, i.e., the trapping force, and (3) the local density of MTs (with time). Therefore, as long as any attractive force exists between the like-charged MTs, the presented experimental configuration may be very efficient to control and promote MT condensation. However, the origin of the attractive force in our experiments with MTs in a typical buffer solution (see Sec. II) remains unclear. In other works, additional macromolecules, such as motor proteins[46,47] and globular polymers,[48,49] are involved in binding MTs in a bundle by either using the specific binding mechanism (the former) or controlling the entropy landscape (the latter). It is reasonable to find the origin from the mechanism of the counterion-induced attractive interaction between like-charged polyelectrolytes as it successfully explains the case of cytoskeletal filaments.[50–54] Moreover, the coupling kinetics obtained from a simulation study on actin filaments[54] is quite similar to what we observe in our experimental study. However, the high ion concentration and the high valency of the ions generally required for the counterion-assisted aggregation are still far removed from our experimental situation. Neither 1 mM $MgCl_2$ nor monovalent salt, which we can find from the buffer solution, was sufficient to observe MT bundles in previous studies.[50,52] The direct electrostatic interaction between MTs, which has been theoretically estimated treating MTs as ordered electrets,[26] may be relevant as it may support the long range spiral order experimentally observed in a MT-crowded system.[55] Additionally, local electric fields produced by micro/nano-wire electrodes may work as external control parameters in the study of phase transitions.[56]

IV. CONCLUSIONS

In summary, we have elucidated that a free-standing wire-type electrode with several micrometers width is capable of spatio-temporal manipulations of MTs under physiological conditions. We performed fluorescence microscopy of rhodamine-labeled MTs to demonstrate electrical control of the distribution of MTs in solution. DC-electric fields generated by using a Pd-MG microwire intensify the density of MTs along the wire. Casein coating of the electrode suppresses the permanent grafting of MTs to the electrode, allowing reversible control of the local density of MTs. MTs are preferentially oriented along the axial direction of the wire during the electric field-induced migration. Reduction of the wire dimensions to a regime comparable with the size of the bio-molecules, multiple arrays or networks of the wires, and simulation studies to determine proper excitations balancing the complex force fields in the ionic medium may open more controllable avenues to regulate the bio-motility system for molecular delivery, sorting, and assembly. Moreover, the ability to organize substances in a three-dimensional system is of general importance. The flexible cylindrical geometry of the electrode may allow a unique external force condition in fundamental research, such as electric field-induced assembly of charged rod-like elements and artificial cellular structures. The electric field-induced MT condensation presented in this work constitutes a preliminary result of this type. Generally, artificial micro/nano-structures producing local electromagnetic fields at a proper length scale embody a rational strategy for the study of interactions between charged cellular elements and local electromagnetic fields, which are ubiquitous in living cellular systems and potentially relevant to diseases like cancer and Alzheimer's disease.[38,39]

ACKNOWLEDGMENTS

We gratefully acknowledge support from the World Premier International Research Center Initiative (WPI), MEXT, Japan. K.S.N. thanks JSPS for KAKENHI Grant No. 25286019.

[1]A. Desai and T. J. Mitchison, Annu. Rev. Cell Dev. Biol. **13**, 83 (1997).
[2]N. Hirokawa, Y. Noda, Y. Tanaka, and S. Niwa, Nat. Rev. Mol. Cell Biol. **10**, 682 (2009).
[3]R. D. Vale, B. J. Schnapp, T. S. Reese, and M. P. Sheetz, Cell **40**, 559 (1985).
[4]R. D. Vale, T. S. Reese, and M. P. Sheetz, Cell **42**, 39 (1985).
[5]M. G. L. van den Heuvel and C. Dekker, Science **317**, 333 (2007).
[6]A. Agarwal and H. Hess, Prog. Polym. Sci. **35**, 252 (2010).
[7]F. J. Nedelec, T. Surrey, A. C. Maggs, and S. Leibler, Nature **389**, 305 (1997).
[8]V. Schaller, C. Weber, C. Semmrich, E. Frey, and A. R. Bausch, Nature **467**, 73 (2010).
[9]Y. Sumino, K. H. Nagai, Y. Shitaka, D. Tanaka, K. Yoshikawa, H. Chaté, and K. Oiwa, Nature **483**, 448 (2012).
[10]T. Sanchez, D. T. N. Chen, S. J. DeCamp, M. Heymann, and Z. Dogic, Nature **491**, 431 (2012).
[11]A. Priel, A. J. Ramos, J. A. Tuszynski, and H. F. Cantiello, Biophys. J. **90**, 4639 (2006).
[12]S. Sahu, S. Ghosh, K. Hirata, D. Fujita, and A. Bandyopadhyay, Appl. Phys. Lett. **102**, 123701 (2013).
[13]H. Hess, J. Clemmens, D. Qin, J. Howard, and V. Vogel, Nano Lett. **1**, 235 (2001).
[14]Y. Hiratsuka, T. Tads, K. Oiwa, T. Kanayama, and T. Q. P. Uyeda, Biophys. J. **81**, 1555 (2001).
[15]J. Clemmens, H. Hess, R. Lipscomb, Y. Hanein, K. F. Böhringer, C. M. Matzke, G. D. Bachand, B. C. Bunker, and V. Vogel, Langmuir **19**, 10967 (2003).
[16]L. J. Cheng, M. T. Kao, E. Meyhofer, and L. J. Guo, Small **1**, 409 (2005).
[17]M. G. L. van den Heuvel, M. P. de Graaff, and C. Dekker, Science **312**, 910 (2006).
[18]R. Yokokawa, Y. Yoshida, S. Takeuchi, T. Kon, and H. Fujita, Nanotechnology **17**, 289 (2006).
[19]R. Stracke, K. J. Böhm, L. Wollweber, J. A. Tuszynski, and E. Unger, Biochem. Biophys. Res. Commun. **293**, 602 (2002).
[20]M. G. L. van den Heuvel, M. P. de Graaff, S. G. Lemay, and C. Dekker, Proc. Natl. Acad. Sci. U.S.A. **104**, 7770 (2007).
[21]L. Jia, S. G. Moorjani, T. N. Jackson, and W. O. Hancock, Biomed. Microdevices **6**, 67 (2004).
[22]I. Minoura and E. Muto, Biophys. J. **90**, 3739 (2006).
[23]M. Uppalapati, Y. M. Huang, T. N. Jackson, and W. O. Hancock, Small **4**, 1371 (2008).
[24]E. Nogales, M. Whittaker, R. A. Milligan, and K. H. Downing, Cell **96**, 79 (1999).
[25]D. Chretien, S. D. Fuller, and E. Karsenti, J. Cell Biol. **129**, 1311 (1995).
[26]J. A. Tuszynski, J. A. Brown, E. Crawford, E. J. Carpenter, M. L. A. Nip, J. M. Dixon, and M. V. Sataric, Math. Comput. Model. **41**, 1055 (2005).
[27]J. A. Noel, W. Teizer, and W. Hwang, ACS Nano **3**, 1938 (2009).
[28]M. G. L. van den Heuvel, C. T. Butcher, S. G. Lemay, S. Diez, and C. Dekker, Nano Lett. **5**, 235 (2005).
[29]E. Kim, K. E. Byun, D. S. Choi, D. J. Lee, D. H. Cho, B. Y. Lee, H. Yang, J. Heo, H. J. Chung, S. Seo, and S. Hong, Nanotechnology **24**, 195102 (2013).
[30]A. Sikora, J. Ramón-Azcón, K. Kim, K. Reaves, H. Nakazawa, M. Umetsu, I. Kumagai, T. Adschiri, H. Shiku, T. Matsue, W. Hwang, and W. Teizer, Nano Lett. **14**, 876 (2014).
[31]K. Kim, A. Liao, A. Sikora, D. Oliveira, M. Umetsu, I. Kumagai, T. Adschiri, W. Hwang, and W. Teizer, Biomed. Microdevices **16**, 501 (2014).
[32]K. Kim, A. Sikora, K. S. Nakayama, H. Nakazawa, M. Umetsu, W. Hwang, and W. Teizer, Appl. Phys. Lett. **105**, 143701 (2014).
[33]K. S. Nakayama, Y. Yokoyama, T. Ono, M. W. Chen, K. Akiyama, T. Sakurai, and A. Inoue, Adv. Mater. **22**, 872 (2010).
[34]K. S. Nakayama, Y. Yokoyama, T. Wada, N. Chen, and A. Inoue, Nano Lett. **12**, 2404 (2012).
[35]P. Kang, X. Serey, Y. F. Chen, and D. Erickson, Nano Lett. **12**, 6400 (2012).
[36]E. W. Dent, J. L. Callaway, G. Szebenyi, P. W. Baas, and K. Kalil, J. Neurosci. **19**, 8894 (1999).
[37]H. H. Gerdes and R. N. Carvalho, Curr. Opin. Cell. Biol. **20**, 470 (2008).
[38]J. Pokorny, A. Foletti, J. Kobilkova, A. Jandova, J. Vrba, J. Vrba, Jr., M. Nedbalova, A. Cocek, A. Danani, and J. A. Tuszynski, Sci. World J. **2013**, 195028.
[39]B. J. Blanchard, B. R. Stockwell, and V. M. Ingram, Biochem. Biophys. Res. Commun. **293**, 1204 (2002).
[40]A. Maloney, L. J. Herskowitz, and S. J. Koch, PLoS One **6**, e19522 (2011).
[41]J. Vanderlinde, *Classical Electromagnetic Theory* (John Wiley & Sons, Inc., New York, 1993), pp. 141–144.
[42]L. K. Ista, G. P. Lopez, C. F. Ivory, M. J. Oritz, T. A. Schifani, C. D. Schwappach, and S. S. Sibbett, Lab Chip **3**, 266 (2003).
[43]M. Stelzle, M. Dürr, M. Cieplik, and W. Nisch, Fresenius J. Anal. Chem. **371**, 112 (2001).
[44]V. VanBauren, D. J. Odde, and L. Cassimeris, Proc. Natl. Acad. Sci. U.S.A. **99**, 6035 (2001).
[45]D. Sept, N. A. Baker, and J. A. Mccammon, Protein Sci. **12**, 2257 (2003).
[46]C. Hentrich and T. Surrey, J. Cell Biol. **189**, 465 (2010).
[47]T. Sanchez, D. Welch, D. Nicastro, and Z. Dogic, Science **333**, 456 (2011).
[48]D. J. Needleman, M. A. Ojeda-Lopez, U. Raviv, K. Ewert, J. B. Jones, H. P. Miller, L. Wilson, and C. R. Safinya, Phys. Rev. Lett. **93**, 198104 (2004).
[49]A. W. C. Lau, A. Prasad, and Z. Dogic, Europhys. Lett. **87**, 48006 (2009).
[50]J. X. Tang, S. Wong, P. T. Tran, and P. A. Janmey, Ber. Bunsenges Phys. Chem. **100**, 796 (1996).
[51]N. Grønbech-Jensen, R. J. Mashl, R. F. Bruinsma, and W. M. Gelbart, Phys. Rev. Lett. **78**, 2477 (1997).
[52]D. J. Needleman, M. A. Ojeda-Lopez, U. Raviv, H. P. Miller, L. Wilson, and C. R. Safinya, Proc. Natl. Acad. Sci. U.S.A. **101**, 16099 (2004).
[53]G. H. Lai, R. Coridan, O. V. Zribi, R. Gloestanian, and G. C. L. Wong, Phys. Rev. Lett. **98**, 187802 (2007).
[54]H. Fazli, S. Mohammadinejad, and R. Golestanian, J. Phys.: Condens. Matter **21**, 424111 (2009).
[55]K. Shigehara, H. Kudoh, S. Mori, Y. Tamura, A. Kakugo, R. Kawamura, H. Furukawa, J. P. Gong, H. Masunage, T. Masui, S. Koizumi, and K. Shikinaka, Soft Matter **8**, 11544 (2012).
[56]A. L. Hitt, A. R. Cross, and R. C. Williams, Jr., J. Biol. Chem. **265**, 1639 (1990).